CELL BIOLOGY

Inhibition of mitochondrial permeability transition by deletion of the ANT family and CypD

Jason Karch[1,2*†], Michael J. Bround[1*], Hadi Khalil[1], Michelle A. Sargent[1], Nadina Latchman[3], Naohiro Terada[4], Pablo M. Peixoto[3], Jeffery D. Molkentin[1,5†]

Copyright © 2019 The Authors, some rights reserved; exclusive licensee American Association for the Advancement of Science. No claim to original U.S. Government Works. Distributed under a Creative Commons Attribution NonCommercial License 4.0 (CC BY-NC).

The mitochondrial permeability transition pore (MPTP) has resisted molecular identification. The original model of the MPTP that proposed the adenine nucleotide translocator (ANT) as the inner membrane pore-forming component was challenged when mitochondria from *Ant1/2* double null mouse liver still had MPTP activity. Because mice express three *Ant* genes, we reinvestigated whether the ANTs comprise the MPTP. Liver mitochondria from *Ant1*, *Ant2*, and *Ant4* deficient mice were highly refractory to Ca^{2+}-induced MPTP formation, and when also given cyclosporine A (CsA), the MPTP was completely inhibited. Moreover, liver mitochondria from mice with quadruple deletion of *Ant1*, *Ant2*, *Ant4,* and *Ppif* (cyclophilin D, target of CsA) lacked Ca^{2+}-induced MPTP formation. Inner-membrane patch clamping in mitochondria from *Ant1*, *Ant2,* and *Ant4* triple null mouse embryonic fibroblasts showed a loss of MPTP activity. Our findings suggest a model for the MPTP consisting of two distinct molecular components: The ANTs and an unknown species requiring CypD.

INTRODUCTION

Mitochondrial permeability transition pore (MPTP) opening contributes to various pathologies involving necrotic cell death after ischemic injuries or degenerative muscle and brain diseases (*1*–*5*). The MPTP occurs within the inner mitochondrial membrane where it is permeable to solutes of up to 1.5 kDa, and it opens in the presence of high matrix Ca^{2+} and/or reactive oxygen species (*6*, *7*). Although numerous regulators of the MPTP have been identified, the molecular pore-forming component of the MPTP remains uncertain (*8*, *9*). Halestrap and Davidson (*10*) first proposed that the adenine nucleotide translocator (ANT) family of genes could serve as the MPTP in 1990, which was consistent with the known effect of ANT ligands and inhibitors on MPTP activity or the fact that reconstituted ANT protein in lipid bilayers formed channel properties similar to the MPTP (*11*–*16*). However, this model was challenged by the report that mouse liver mitochondria lacking the genes *Ant1* and *Ant2* still underwent mitochondrial permeability transition (MPT), albeit at substantially higher levels of Ca^{2+} (*17*). Here, we investigated whether the third *Ant* gene in mice, *Ant4*, compensates for the loss of *Ant1* and *Ant2* and whether mitochondria completely null for all ANT isoforms would undergo MPT [humans contain four *Ant* genes (*Ant1* to *Ant4*), while mice lack *Ant3*] (*18*). More recently, a model in which the mitochondrial F_1F_O ATP synthase (ATPase) serves as the MPTP was proposed (*19*–*21*), although not without controversy as some data dispute this model (*22*–*24*).

RESULTS

We first characterized the tissue distribution of all three ANT isoforms in the mouse by Western blotting from mitochondria lysates. In wild-type (WT) mice, ANT1 is the major isoform expressed in the heart and skeletal muscle, while ANT2 is expressed in all tissues examined besides the testis, the latter of which predominantly expresses ANT4 (Fig. 1A). Of the three ANT isoforms, mouse liver predominantly expresses ANT2 at baseline (Fig. 1A). In mice globally lacking either *Ant1* or *Ant4*, the ANT2 isoform becomes upregulated to compensate for their loss (Fig. 1A). We observed that ANT4 expression is induced in liver mitochondria from mice lacking *Ant1* and *Ant2* (Fig. 1, B and C). This observation of compensation by ANT4 when *Ant1* and *Ant2* were deleted from the liver likely explains why Kokoszka and colleagues (*17*) failed to observe a more severe loss of MPTP activity. The *Ant2* gene was LoxP-targeted to permit tissue-specific deletion, because full somatic $Ant2^{-/-}$ mice are embryonic lethal (*25*).

Here, we generated mice null for all ANT isoforms in the liver by crossing total somatic $Ant1^{-/-}$, $Ant4^{-/-}$ with *Ant2-LoxP* (*fl*) mice with an albumin promoter–driven Cre transgenic mouse line ($Ant2^{fl/fl\text{-}Alb\text{-}Cre}$) (*17*, *26*). The loss of all ANT isoform expression in the liver was confirmed by Western blot analysis on isolated liver mitochondria (Fig. 1, D and E). In all liver-based experiments, $Ant1^{-/-}$ $Ant4^{-/-}$ $Ant2^{fl/fl}$ mice were used as controls, because ANT2 is the overwhelming isoform expressed in liver (Fig. 1, A and D). This strategy allowed us to directly compare littermates ($Ant1^{-/-}$ $Ant4^{-/-}$ $Ant2^{fl/fl\text{-}Alb\text{-}Cre}$ versus $Ant1^{-/-}$ $Ant4^{-/-}$ $Ant2^{fl/fl}$). Tetramethylrhodamine ethyl ester (TMRE) staining showed comparable membrane potential that was sensitive to carbonyl cyanide *p*-trifluoromethoxyphenylhydrazone (FCCP) treatment in mitochondria from $Ant1^{-/-}$ $Ant4^{-/-}$ $Ant2^{fl/fl\text{-}Alb\text{-}Cre}$ (*Ant*-triple-null) livers and the ANT2-only expressing mice ($Ant1^{-/-}$ $Ant4^{-/-}$ $Ant2^{fl/fl}$; ANT2-only) (Fig. 1F). Hematoxylin and eosin (H&E)–stained histological liver sections and transmission electron microscopy also showed no overt pathology in *Ant*-triple-null versus ANT2-only expressing mice (fig. S1A). In an unexpected deviation from previous work (*17*), *Ant*-triple-null mitochondria from liver showed no difference in adenosine diphosphate (ADP)–stimulated and maximum oxygen consumption rates and no decrease in ATP levels when compared with ANT2-only controls, suggesting that ANT function is somehow compensated for in these mitochondria, presumably by another *Slc25a* family member (figs. S1B and S2, A to C).

[1]Department of Pediatrics, Cincinnati Children's Hospital and University of Cincinnati, Cincinnati, OH, USA. [2]Department of Molecular Physiology and Biophysics, Cardiovascular Research Institute, Baylor College of Medicine, Houston TX, USA. [3]Baruch College and Graduate Center of City University of New York, NY, USA. [4]Department of Pathology, University of Florida College of Medicine, Gainesville, FL, USA. [5]Howard Hughes Medical Institute, Chevy Chase, MD, USA.
*These authors contributed equally to this work.
†Corresponding author. Email: jeff.molkentin@cchmc.org (J.D.M.); jason.karch@bcm.edu (J.K.)

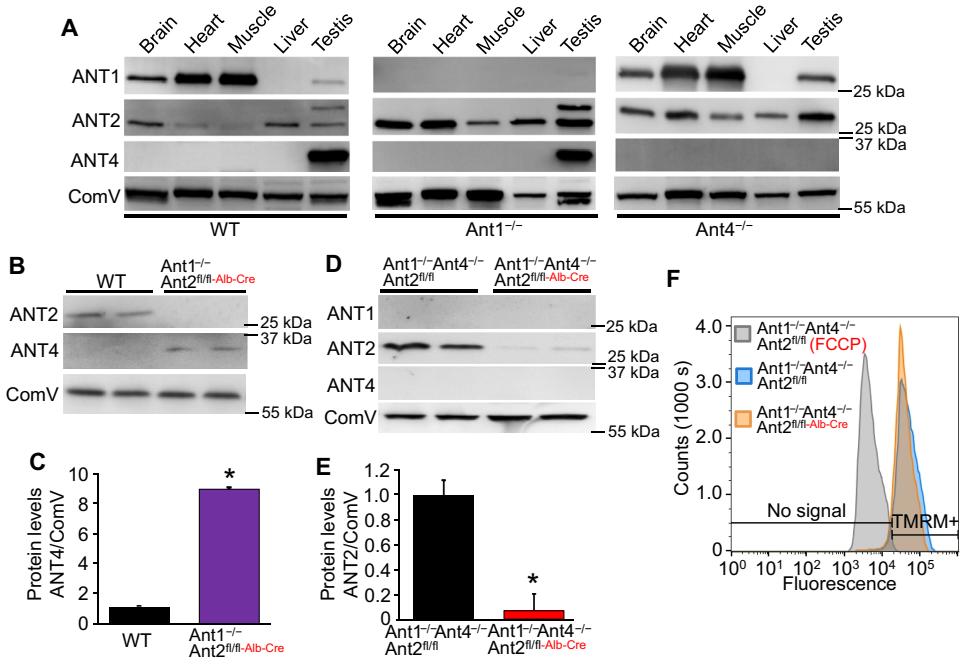

Fig. 1. Tissue-specific expression and compensation of the ANT family. (**A**) Western blots of isolated mitochondria from various mouse tissues for ANT1, ANT2, ANT4, and a loading control for electron transport chain complex V (ComV). ANT2 protein is up-regulated in all five tissues analyzed to compensate for the loss of the *Ant1* gene. ANT2 is up-regulated in testis in response to loss of the *Ant4* gene. These results are representative of three independent experiments. (**B**) Western blots for ANT2 and ANT4 from isolated liver mitochondria from the indicated gene-targeted mice showing that ANT4 is induced for the first time in the absence of the *Ant1* and *Ant2* genes. A loading control for ComV is shown. These results are representative of three independent experiments. (**C**) Quantification of ANT4 expression normalized to ComV expression, as in (B) ($n = 3$; $^*P \leq 0.05$). (**D**) Western blots of ANT1, ANT2, ANT4, and a loading control for ComV, performed using extracts of isolated liver mitochondria from *Ant1*$^{-/-}$ *Ant4*$^{-/-}$ *Ant2*$^{fl/fl}$ (ANT2-only) and *Ant1*$^{-/-}$ *Ant4*$^{-/-}$ *Ant2*$^{fl/fl\text{-}Alb\text{-}Cre}$ (*Ant*-triple-null) mice. Data are representative of three independent experiments. (**E**) Quantification of ANT2 expression normalized to ComV expression, as in (D) ($n = 4$; $^*P \leq 0.05$). (**F**) Representative fluorescence-activated cell sorting analysis of TMRE-stained mouse liver mitochondria isolated from *Ant1*$^{-/-}$ *Ant4*$^{-/-}$ *Ant2*$^{fl/fl}$ versus *Ant1*$^{-/-}$ *Ant4*$^{-/-}$ *Ant2*$^{fl/fl\text{-}Alb\text{-}Cre}$ mice. The TMRE fluorescence threshold is shown in the bottom of the panel versus when no fluorescence signal is detected above background. FCCP is a potent uncoupler of mitochondrial respiration, which is provided to depolarize mitochondria. Results are representative of three independent experiments.

To investigate the status of MPTP activity, we simultaneously used the two most common MPTP assays in isolated mitochondria: that of Ca^{2+} retention capacity (CRC) using stepwise 40 μM Ca^{2+} additions over time and that of absorbance-based assessment of mitochondrial swelling. Mitochondria from WT mouse liver took up three stepwise Ca^{2+} additions before opening and releasing their Ca^{2+} into the solution (Fig. 2A). This Ca^{2+}-induced MPTP opening caused immediate mitochondria swelling in the solution, indicated by a decrease in light absorbance (Fig. 2B). Consistent with previous results (*17*), loss of ANT1 and ANT2 desensitized Ca^{2+}-induced MPTP opening to a similar extent as WT mitochondria treated with cyclosporine A (CsA) (*27*, *28*), which is an inhibitor of the MPTP regulator cyclophilin D (CypD) (Fig. 2, A and B). Mitochondria lacking all isoforms of the ANT family are further desensitized to Ca^{2+}-induced MPTP opening; however, the MPTP still opened with very high levels of Ca^{2+} (Fig. 2, A and B, and fig. S1C), confirming that the ANT family is still dispensable for MPTP opening in the liver. In contrast, *Ant*-triple-null mitochondria that were also treated with CsA showed no mitochondrial swelling despite taking up Ca^{2+} to the physical limits of the assay (4.8 mM Ca^{2+}) (Fig. 2, A and B, and fig. S1C). *Ant*-triple-null mitochondria treated with CsA swelled when treated with the nonspecific permeabilizing agent alamethicin, demonstrating that *Ant*-triple-null mitochondria were otherwise intact and capable of swelling (Fig. 2B, arrowhead).

We observed a similar synergistic effect in the reciprocal experiment when *Ppif*$^{-/-}$ mitochondria lacking CypD were treated with ADP, a known desensitizer of the MPTP and ligand for ANT (Fig. 2, C and D, and fig. S1C). Together, these data reveal that MPTP formation requires at least one ANT family member or CypD to occur. These studies further suggest that there may be at least two separate pores that comprise total MPTP activity in liver: one pore consisting of the ANT family that can escape CypD regulation and another that is dependent on CypD to open.

To further address the data obtained in purified mitochondria with CsA in *Ant*-triple-null mice, we independently generated quadruple-null mice for *Ant1*, *Ant2*, *Ant4*, and *Ppif*. We compared the CRC and swelling measurements in liver mitochondria from these quadruple-null mice versus ANT2-only control mice (Fig. 3, A to C). While ANT2-only mitochondria took up a limited number of 40 μM Ca^{2+} boluses before pore opening and swelling, the quadruple-null never underwent swelling and took up Ca^{2+} boluses until the Ca^{2+} sensing potential of the assay was saturated (Fig. 3, A and B). Electron microscopy showed that liver mitochondria from ANT2-only control mice, *Ant*-triple-null mice, and *Ppif*$^{-/-}$ mice had morphologically normal mitochondria at baseline in Ca^{2+}-free buffer, but after the addition of 800 μM Ca^{2+}, all showed profound swelling (Fig. 3C). Conversely, mitochondria from *Ant1*$^{-/-}$ *Ant4*$^{-/-}$ *Ppif*$^{-/-}$ *Ant2*$^{fl/fl\text{-}Alb\text{-}Cre}$ quadruple-null livers failed to show swelling (Fig. 3C, red arrowheads), despite also using half the amount

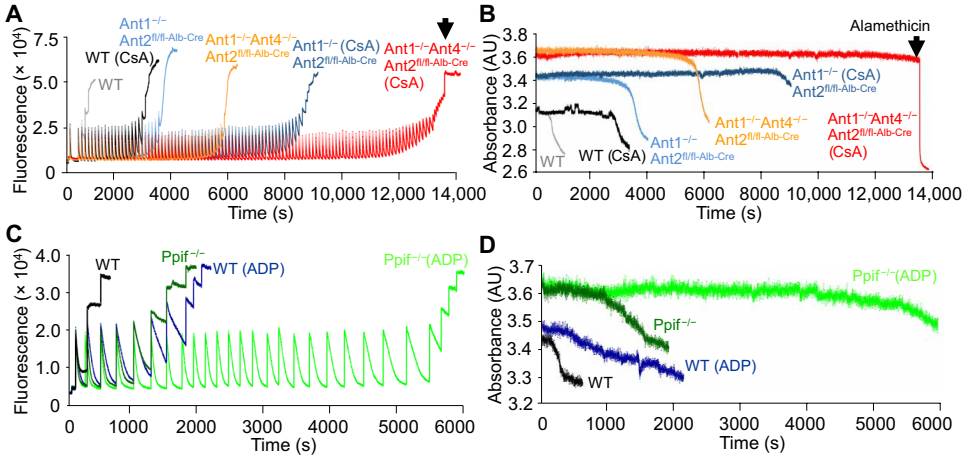

Fig. 2. Loss of the ANT family or CypD desensitizes the MPTP, while *Ant* family deletion with CsA completely inhibits MPTP opening. (**A**) Ca^{2+} retention capacity (CRC) assay with Calcium Green-5N fluorescence indicator in the buffer was performed using purified liver mitochondria isolated from wild-type (WT), *Ant1*$^{-/-}$ *Ant2*$^{fl/fl\text{-}Alb\text{-}Cre}$, or *Ant1*$^{-/-}$ *Ant4*$^{-/-}$ *Ant2*$^{fl/fl\text{-}Alb\text{-}Cre}$ mice treated with or without 5 μM cyclosporine A (CsA). Two milligrams of mitochondria were used in each assay, and 40 μM pulses of $CaCl_2$ were continually given (represented by each peak in fluorescence in the traces) until mitochondria either underwent MPTP or displayed saturated Ca^{2+} uptake. The arrowhead shows 40 μM alamethicin addition, a membrane-permeabilizing agent. (**B**) Simultaneous with the CRC assay shown in (A), light absorbance was recorded during the course of Ca^{2+} additions to measure mitochondrial swelling represented by a decrease in absorbance. The results shown are representative traces from at least three independent assays. AU, arbitrary units. (**C**) CRC assay using conditions similar to those of (A) performed on liver mitochondria isolated from WT or *Ppif*$^{-/-}$ mice treated with or without 50 μM ADP. (**D**) Absorbance-based mitochondria swelling was simultaneously measured in the CRC assay samples shown in (C). The results shown are representative traces from at least three independent assays.

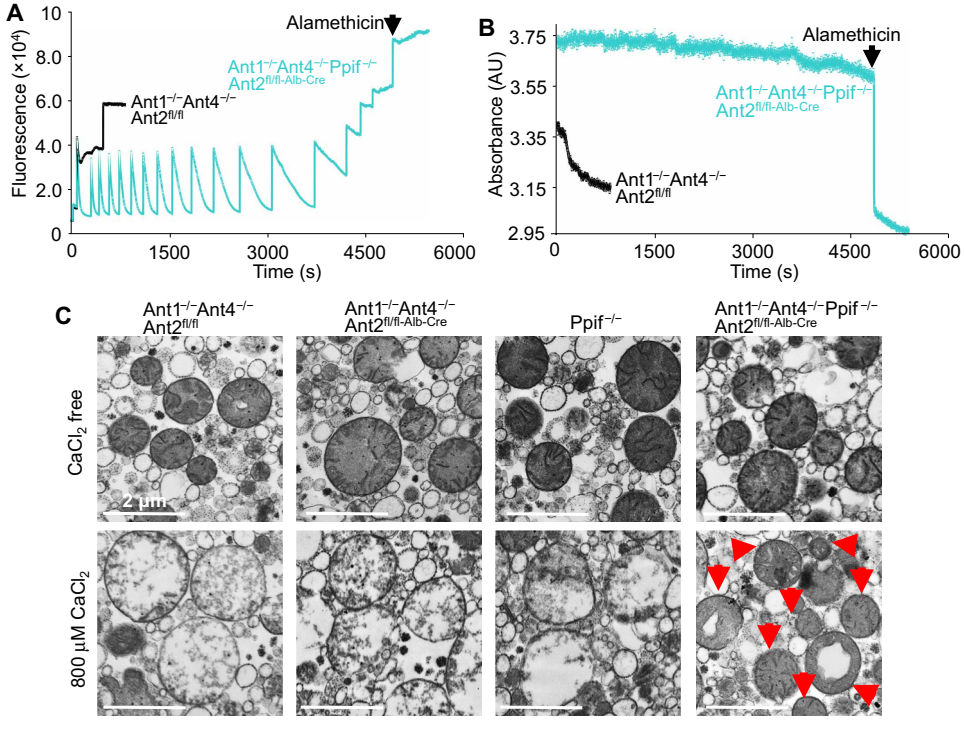

Fig. 3. Genetic deletion of the *Ant* family and *Ppif* completely inhibits MPTP opening. (**A**) CRC assay performed in purified liver mitochondria isolated from *Ant1*$^{-/-}$ *Ant4*$^{-/-}$ *Ant2*$^{fl/fl}$ (ANT2-only) or *Ant1*$^{-/-}$ *Ant4*$^{-/-}$ *Ppif*$^{-/-}$ *Ant2*$^{fl/fl\text{-}Alb\text{-}Cre}$ (quadruple-null) mice. Two milligrams of mitochondria per assay were used, and 40 μM pulses of $CaCl_2$ were continually given until mitochondrial Ca^{2+} uptake no longer occurred or the mitochondria underwent MPT as evidenced by irreversible increase in Calcium Green-5N fluorescence, which was saturated in the presence of 40 μM alamethicin (arrowhead). Similar results were observed across three independent assays. (**B**) Simultaneous with the CRC assay shown in (A), light absorbance was recorded during the course of Ca^{2+} additions to measure mitochondrial swelling represented by a decrease in absorbance. The results shown are representative traces from at least three independent assays. (**C**) Electron microscopy images of isolated liver mitochondria treated with or without 800 μM $CaCl_2$ from *Ant1*$^{-/-}$ *Ant4*$^{-/-}$ *Ant2*$^{fl/fl}$ (ANT2-only controls), *Ant1*$^{-/-}$ *Ant4*$^{-/-}$ *Ant2*$^{fl/fl\text{-}Alb\text{-}Cre}$ (*Ant*-triple-null), and *Ppif*$^{-/-}$, and *Ant1*$^{-/-}$ *Ant4*$^{-/-}$ *Ppif*$^{-/-}$ *Ant2*$^{fl/fl\text{-}Alb\text{-}Cre}$ (quadruple-null) mice. The red arrowheads show quadruple-null mitochondria that were refractory to swelling after treatment with 800 μM $CaCl_2$. Representative images that are consistent across all fields analyzed from two independent isolations are shown.

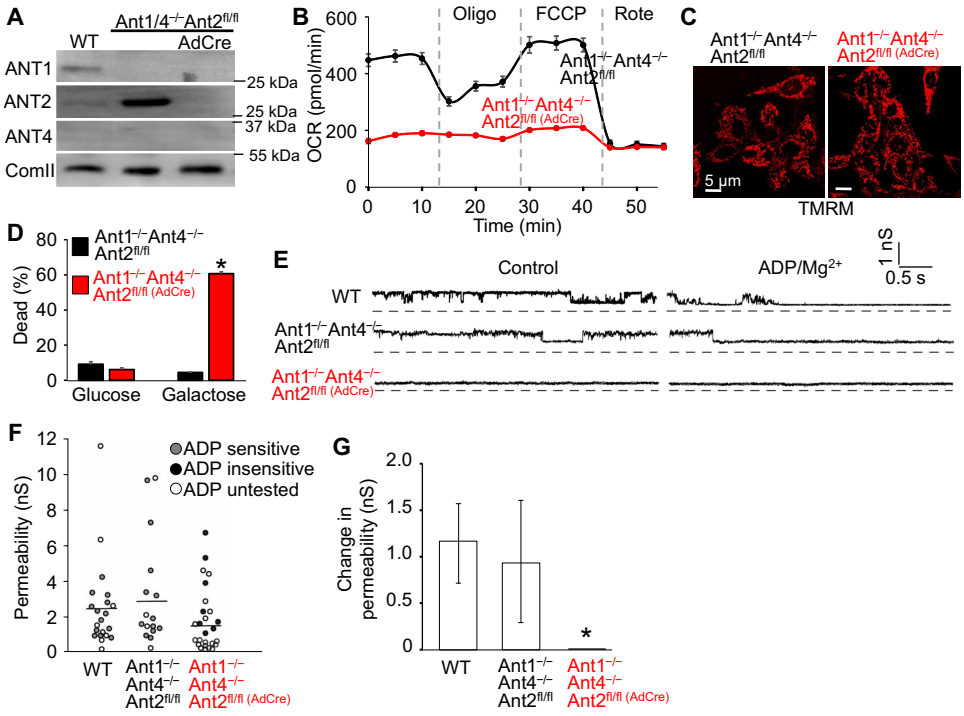

Fig. 4. The ANT family is the pore-forming component of the MPTP in MEFs. (**A**) Western blots of ANT1, ANT2, ANT4, and complex II (ComII) loading control from extracts of isolated mitochondria from MEFs that are WT or *Ant1*$^{-/-}$ *Ant4*$^{-/-}$ *Ant2*$^{fl/fl}$ that have been treated with or without adenovirus-expressing Cre recombinase (AdCre will delete *Ant2*). (**B**) Oxygen consumption rate (OCR) of stable MEF lines that were *Ant1*$^{-/-}$ *Ant4*$^{-/-}$ *Ant2*$^{fl/fl}$ (ANT2-only) versus *Ant1*$^{-/-}$ *Ant4*$^{-/-}$ *Ant2*$^{fl/fl(AdCre)}$ (*Ant*-triple-null) ($n = 5$). Respiration was challenged with sequential treatment of 2 μM oligomycin (Oligo), 2 μM FCCP, and 0.5 μM rotenone (Rote) ($n = 5$). (**C**) Confocal microscopic images of TMRE staining of the same MEF lines described in (B). Similar profiles of TMRE fluorescence were observed in three independent experiments. (**D**) Cell death analysis of the *Ant*-triple-null MEFs versus the *Ant1*$^{-/-}$ *Ant4*$^{-/-}$ *Ant2*$^{fl/fl}$ (ANT2-only) controls, subjected to glucose-containing (normal) media or glucose-free, galactose-containing media for 24 hours. Cell death was determined by loss of plasma membrane integrity ($n = 3$; *$P \leq 0.05$). (**E**) Representative patch clamp current traces of mitoplasts isolated from the MEFs described in (A) in the presence of 250 μM $CaCl_2$. The high conductance openings in the WT and ANT2-only lines were sensitive to the addition of 1 mM ADP/Mg^{2+} (right). (**F**) Scatterplot of the permeability in nanosiemens (nS) from all recorded patches. The number of patches analyzed is represented by the data plots (circles). The horizontal lines indicate average permeability. Solid circles represent channels that were either sensitive (gray) or insensitive (black) to the addition of 1 mM ADP/$MgCl_2$ [WT versus *Ant1*$^{-/-}$ *Ant4*$^{-/-}$ *Ant2*$^{fl/fl(AdCre)}$, $P = 0.069$]. Open circles represent ADP response untested. (**G**) Bar histograms of average (±SD) change in permeability after bath perfusion with 1 mM ADP/$MgCl_2$ [WT, $n = 13$; *Ant1*$^{-/-}$ *Ant4*$^{-/-}$ *Ant2*$^{fl/fl}$, $n = 12$; *Ant1*$^{-/-}$ *Ant4*$^{-/-}$ *Ant2*$^{fl/fl(AdCre)}$, $n = 8$; *$P \leq 0.05$].

of mitochondria (1 mg versus 2 mg) to correct for baseline absorbance differences (fig. S3A). Similar to the *Ant*-triple-null mitochondria, *Ant1*$^{-/-}$ *Ant4*$^{-/-}$ *Ppif*$^{-/-}$ *Ant2*$^{fl/fl\text{-}Alb\text{-}Cre}$ quadruple-null mitochondria displayed no alteration in morphology or stimulated oxygen consumption under energized conditions (fig. S3, B and C).

To extend these findings to another model system, we also generated mouse embryonic fibroblasts (MEFs) lacking all ANT isoforms (Fig. 4A). In contrast to the liver mitochondria, mitochondria isolated from *Ant1*$^{-/-}$ *Ant4*$^{-/-}$ *Ant2*$^{fl/fl\text{-}(AdCre)}$ MEFs (*Ant*-triple-null) did not show compensation in their ability to transport ATP/ADP so that these mitochondria had almost no respiratory capacity and reduced ATP levels with increased ADP (Fig. 4B and fig. S2, D to F). The relative increase in ADP may contribute to MPTP desensitization in these mitochondria from *Ant*-triple-null MEFs. To explore whether *Ant*-triple-null MEFs depend on glycolysis to generate ATP, we grew them in glucose-free, galactose-containing culture media, making glycolysis an ATP futile process. Under these conditions, the *Ant*-triple-null MEFs died within 24 hours, whereas the control MEFs were unaffected (Fig. 4D). We observed similar cell death in *Ant*-triple-null MEFs within 12 hours of treatment with 40 mM 2-deoxygluose, a potent inhibitor of glycolysis. Despite reduced mitochondrial respiration, *Ant*-triple-null MEFs were still capable of generating mitochondrial membrane potential ($\Delta\Psi$) in culture, as measured by TMRE fluorescence (Fig. 4C), presumably from pyruvate and reducing equivalents generated from glycolysis.

We also assessed MPTP activity by patch clamping of the inner mitochondrial membrane to identify its known opening and conductance properties. Mitoplasts isolated from WT and ANT2-only MEFs (*Ant1*$^{-/-}$ *Ant4*$^{-/-}$ *Ant2*$^{fl/fl}$) showed channel opening and conductance levels consistent with the MPTP, and importantly, ADP, an MPTP suppressor, inhibited pore opening events (Fig. 4, E and F). Patching of mitoplasts from *Ant*-triple-null MEFs showed a much lower prevalence of large pores, and all such rare pores were unresponsive to ADP, suggesting that no MPTP-like channels were present without ANT (Fig. 4, E and G). These results suggest that the ANT family is the primary inner-membrane channel-forming component of the MPTP in MEFs.

DISCUSSION

In summary, we have genetically abolished MPT by deletion of the ANT family and CypD in liver mitochondria, validating the original model proposed for this phenomenon. However, in liver mitochondria, our data support a "multi-pore model" where the MPTP is composed of at least two distinct molecular components, one of which

is ANT and the other depends on CypD (fig. S4). In these mitochondria, the ANT-dependent MPT activity, while likely regulated by CypD, is able to activate independently of CypD in response to higher mitochondrial matrix Ca^{2+} levels. Meanwhile, the second, unknown MPTP component requires the presence of CypD and cannot activate in its absence. The possibility that the MPTP is composed of at least two pore-forming components may explain why identifying its gene products has been controversial. However, it is also possible that CypD and the ANTs activate a still unknown common pore in a "dual regulator model." In this situation, the MPTP is regulated by ANTs and CypD that can function independently. Our data suggest that this hypothetical common pore requires at least CypD or the ANTs to activate and that both regulators must be disrupted to silence the MPTP. Despite this possibility, MEFs lacking all three *Ant* genes completely lack MPTP activity, suggesting that ANT directly constitutes the fundamental unit of pore activity in select cell types. In moving forward, it will be important to identify the additional unknown CypD-dependent component of the MPTP in the liver. For example, other *Slc25a* family members, such as the *Slc25a3* (mitochondrial phosphate carrier), or the mitochondrial F_1F_O ATPase could fulfill such a role (*19*–*21*, *29*, *30*).

MATERIALS AND METHODS

Animal models

Ant1$^{-/-}$ (*Slc25a4*) *Ant2-LoxP* (*fl*) (*Slc25a5*) mice and *Ant4*$^{-/-}$ (*Slc25a31*) mice were described previously (*16*, *17*). To generate liver-specific deletion *Ant2*$^{fl/fl}$ in mice, we crossed in an albumin-Cre transgenic line (the Jackson Laboratory, 003574). To delete the CypD gene product, we used mice lacking a functional *Ppif* gene (*27*). *Ppif*$^{-/-}$ mice were crossed to contain the *Ant1*$^{-/-}$ *Ant4*$^{-/-}$ and *Ant2*$^{fl/fl\text{-}Alb\text{-}Cre}$ alleles to generate quadruple gene-deleted mice. *Ant*-triple-null liver was generated in *Ant1*$^{-/-}$ *Ant4*$^{-/-}$ *Ant2*$^{fl/fl\text{-}Alb\text{-}Cre}$ mice, which were compared with *Ant1*$^{-/-}$ *Ant4*$^{-/-}$ and *Ant2*$^{fl/fl}$ littermates that lacked the albumin-Cre transgene, and hence, these mice only expressed ANT2 (ANT2-only), which is the predominant ANT family member normally expressed in liver. However, liver mitochondria from ANT2-only mice showed identical mitochondrial CRC and Ca^{2+}-induced swelling to fully WT mitochondria. Moreover, mitochondrial ultrastructure in liver from neither *Ppif*$^{-/-}$ nor *Ant1*$^{-/-}$ *Ant4*$^{-/-}$ *Ant2*$^{fl/fl\text{-}Alb\text{-}Cre}$ mice showed alterations compared with WT mitochondria (see fig. S3C).

All experimental procedures with animals were approved by the Institutional Animal Care and Use Committee of Cincinnati Children's Medical Center, protocols IACUC 2015-0047 and 2016-0069. We have complied with the relevant ethical considerations for animal usage overseen by this committee. The number of mice used in this study reflects the minimum number needed to achieve statistical significance based on experience and previous power analysis. Blinding was performed for some experimental procedures with mice, although blinding was not possible in every instance. Both sexes of mice were used in equal ratios.

Cell culture models

MEFs were generated by harvesting *Ant1*$^{-/-}$ *Ant2*$^{fl/fl}$ *Ant4*$^{-/-}$ embryonic day 10.5 embryos. After the removal of the internal organs and the head, the remainder of the bodies were passed through a 25-gauge needle and plated on 10-cm^2 tissue culture dishes and cultured in Dulbecco's modified Eagle's medium (DMEM) (Thermo Fisher Scientific) containing 10% bovine growth serum (BGS, Thermo Fisher Scientific), penicillin-streptomycin (Thermo Fisher Scientific), and nonessential amino acids (Invitrogen). After two passages, the MEFs were subjected to simian virus 40 (SV40) large T antigen immortalization by infecting with an SV40 T antigen–expressing lentivirus (Addgene, plasmid 22298, pLenti CMV/TO SV40 small + large T). Once immortalization was achieved, cells were treated with an adenovirus expressing both green fluorescent protein (GFP) and Cre recombinase (AdCre) for *Ant2* gene deletion. Before infection, these MEFs were switched to "Rho 0" medium, which was the standard DMEM described above supplemented with uridine (50 μg/ml; Sigma-Aldrich) and 1 mM sodium pyruvate (Thermo Fisher Scientific). After infection, MEFs were subjected to fluorescent-activated cell sorting to isolate individual GFP-positive cells that had AdCre virus infection, which established clonal *Ant*-triple-null MEFs. Validation of the loss of ANT2 protein was determined by Western blot analysis. After cell selection, we were able to culture *Ant*-deleted MEF lines in high-glucose DMEM (4.5 g/liter glucose; Thermo Fisher Scientific) supplemented with 10% BGS (Thermo Fisher Scientific) and nonessential amino acids (Invitrogen). To determine if the *Ant*-triple-null MEFs relied on mitochondria-produced ATP for survival, we cultured the MEFs in glucose-free media (Thermo Fisher Scientific) with the addition of galactose (4500 mg/ml; Sigma-Aldrich), which caused their death within 24 hours, as measured with the Muse Cell Analyzer (MilliporeSigma) and the Muse Count & Viability Assay Kit (MilliporeSigma). To further test ANT MEF reliance on glycolysis, we treated cells cultured in Rho 0 media containing 40 mM 2-deoxyglucose (Sigma-Aldrich). Cells were visually inspected 12 hours later for survival.

Mitochondrial isolation

The brain, heart, muscle, liver, testis, and MEF mitochondria were isolated in MS-EGTA buffer [225 mM mannitol, 75 mM sucrose, 5 mM Hepes, and 1 mM EGTA (pH 7.4); Sigma-Aldrich]. The various tissues were minced into 2 mm by 2 mm pieces and then homogenized using a glass and Teflon tissue homogenizer (8 to 15 strokes, depending on the tissue) on ice and in MS-EGTA buffer. Tissue homogenates were then subjected to a 2500*g* centrifugation for 5 min (1×), and the supernatants were then centrifuged at 11,500*g* for 10 min. The MEFs were grown to confluency on four Nunc Bioassay Dishes (Sigma-Aldrich) and then harvested and pelleted in MS-EGTA buffer. The cells were then suspended in 7 ml of buffer and homogenized with a glass and Teflon tissue homogenizer (10 strokes). MEF homogenates were then subjected to a 2500*g* centrifugation for 5 min (2×), and the supernatants were then centrifuged at 11,500*g* for 10 min. In both situations, pellets were then washed and centrifuged 2× (11,500*g*) and then snap-frozen or suspended in KCl buffer [125 mM KCl, 20 mM Hepes, 2 mM $MgCl_2$, 2 mM KH_2PO_4, and 40 μM EGTA (pH 7.2); Sigma-Aldrich].

CRC and mitochondrial swelling assays

The CRC assay and the mitochondrial swelling assay were performed simultaneously using a dual-detector (one to measure fluorescence and the other to measure absorbance), single-cuvette–based fluorimetric system (Horiba Scientific). Depending on the experiment, 1 or 2 mg of isolated mitochondria was loaded into the cuvette along with 250 nM Calcium Green-5N (Invitrogen), 7 mM pyruvate (Sigma-Aldrich), and 1 mM malate (Sigma-Aldrich) and brought up to 1 ml using KCl buffer. Mitochondria were then pulsed with sequential additions of $CaCl_2$ (40 or 800 μM) until MPTP opening

occurred or until the mitochondria reached a $CaCl_2$ saturation point and could no longer take up more Ca^{2+}. In certain situations where the experimental mitochondria did not undergo a swelling event following $CaCl_2$ additions, they would be subjected to a membrane-permeabilizing agent, 40 μM alamethicin (Santa Cruz Biotechnology), to show that they still had swelling capacity and were not otherwise compromised.

TMRE assay

MEFs were plated on glass-bottom tissue culture dishes and loaded with 50 nM TMRE (Thermo Fisher Scientific) for 10 min. Following loading, cells were washed twice with Hanks' balanced salt solution (Thermo Fisher Scientific) and immediately visualized using a Nikon A1 inverted confocal microscope (Nikon) (488 nm excitation/575 nm emission). Isolated liver mitochondria suspended in KCl buffer were loaded with 50 nM TMRE for 10 min and then centrifuged and washed with fresh KCl buffer. The mitochondria were then immediately analyzed by flow cytometry (488 nm excitation/575 nm emission). TMRE positivity was confirmed by treating loaded mitochondria with 5 μM FCCP (Abcam) and recording a large negative shift in the entire mitochondrial population.

Western blotting

All Western blots were performed using isolated mitochondrial lysates. Following mitochondrial isolations, the mitochondrial pellets were suspended in radioimmunoprecipitation buffer containing protease inhibitor cocktails (Roche). The samples were then sonicated, and the insoluble fractions were discarded following centrifugation. SDS sample buffer was added to the lysates, and samples were boiled for 5 min. The samples were then loaded onto 10 to 15% acrylamide gels and then transferred onto polyvinylidene fluoride transfer membranes (MilliporeSigma). The following primary antibodies were used: Slc25a4 (ANT1) (Signalway Antibody; 32484; 1:500), Slc25a5 (ANT2) (Cell Signaling Technology; 14671; 1:500), ANT4 polyclonal antibody (Signalway Antibody; 40596-1; 1:500), and Total OXPHOS rodent WB antibody cocktail (that contained antibodies to complexes 1 to 5, ComII, or ComV as labeled in Western blots) (Abcam; ab110413; 1:15,000).

Metabolic analysis

Oxygen consumption rate was determined using an XF Extracellular Flux Analyzer (Agilent Technologies). MEFs were plated in XF24 microplates (Agilent Technologies) and grown to confluency in Rho 0 media (as described above), and switched to an assay medium composed of Seahorse XF base medium (Agilent Technologies) supplemented with 10 mM glucose (Agilent Technologies), 1 mM pyruvate (Agilent Technologies), and 2 mM L-glutamine (Agilent Technologies), and subjected to the Mito Stress Test Kit (Agilent Technologies) using the standard protocol provided. Briefly, after basal respiration was measured, the MEFs were treated sequentially with 2 μM oligomycin, 2 μM FCCP, and 0.5 μM rotenone. Isolated liver mitochondria (300 μg) were loaded onto XF24 cell culture microplates in KCl buffer containing 7 mM pyruvate and 1 mM malate and subjected to the Mito Stress Test Kit using the standard protocol provided. Briefly, after basal respiration was measured, the mitochondria were treated sequentially with 10 mM ADP, 2 μM oligomycin, 5 μM FCCP, and 0.5 μM rotenone. To interrogate ADP uptake, 200 μg of isolated liver or MEF mitochondria was loaded onto XF24 cell culture microplates in KCl buffer containing 7 mM pyruvate and 1 mM malate and treated sequentially with ascending concentrations of ADP (0.5, 2, and 2.5 mM) followed by 0.5 μM rotenone.

Adenine nucleotide concentrations were measured using chemical assay kits. The Abcam ATP Assay Kit (Abcam) was used to measure mitochondrial ATP levels. Either 2 mg of previously frozen, isolated liver mitochondria or 1 mg of previously frozen, isolated MEF mitochondria was suspended in 100 μl of KCl buffer and diluted with 400 μl of ATP assay buffer. Either 40 μg of liver mitochondria or 20 μg of MEF mitochondria was added to each assay, and ATP levels were measured according to the fluorometric assay protocol. Cell Technology Fluoro ADP^{TM}: fluorescent Cellular and Tissue ADP Detection Kit (Cell Technology) was used to measure mitochondrial ADP levels. Either 2 mg of previously frozen, isolated liver mitochondria or 1 mg of previously frozen, isolated MEF mitochondria was suspended in 100 μl of KCl buffer and diluted with 200 μl of substrate buffer and sonicated for 3 min. One hundred ten micrograms of liver mitochondria or 55 μg of MEF mitochondria was added to each assay, and ADP levels were measured according to the Fluoro ADP Assay protocol (Cell Technology).

Histological analyses

Histological analyses of the H&E-stained slides of 7-μm liver sections were performed using an upright microscope 4× objective. Electron microscopy was performed on livers and isolated mitochondria from livers. Before fixation, the isolated mitochondria were subjected to the mitochondrial swelling assay with or without $CaCl_2$ (two pulses of 400 μM $CaCl_2$ to achieve 800 μM). Samples were then fixed in glutaraldehyde and cacodylate, embedded in epoxy resin, and sectioned. Sections were counterstained with uranyl acetate and lead citrate. Images were taken at 5000× and 3500×.

Patch-clamping techniques

MEFs at 80% confluency were harvested, and mitochondria were isolated as previously described (*31*). Mitoplasts were spontaneously formed by diluting isolated mitochondria 100-fold in patching media (see below) for 10 min, which caused controlled swelling and rupture of the outer membrane. Mitoplasts can be easily distinguished from intact mitochondria, as they appear as larger and more translucent ring-like structures studded by a curled outer membrane. Inner-membrane patches were excised from mitoplasts after formation of a seal using micropipettes with approximately 0.3-μm tips and resistances of 10 to 30 megohms at room temperature. Patching medium was 150 mM KCl, 5 mM Hepes, 1.25 mM $CaCl_2$, and 1 mM EGTA (pH 7.4). Voltages were clamped with a Dagan 1200 amplifier and reported as pipette potentials. Permeability was typically determined from stable current levels and/or total amplitude histograms of 30 s of data at +20 mV. pCLAMP version 8 (Axon Instruments) and WinEDR v2.3.3 (Strathclyde Electrophysiology Software) were used for current analysis as previously described (*32*). Sample rate was 5 kHz with 1- to 2-kHz filtration. To determine whether the large conductance activity was due to the MPTP through the ANT family, patching medium containing 1 mM ADP/$MgCl_2$ was administered by bath perfusion.

SUPPLEMENTARY MATERIALS

Supplementary material for this article is available at http://advances.sciencemag.org/cgi/content/full/5/8/eaaw4597/DC1

Fig. S1. Loss of *Ant1/2/4* genes in the liver does not compromise mitochondrial energetics or cause tissue pathology.

Fig. S2. Adenine nucleotide levels and transport in liver and MEF mitochondria lacking ANT proteins.

Fig. S3. Mitochondria from quadruple null mice fail to undergo Ca^{2+}-induced MPTP, although no defects in energetics or mitochondrial ultrastructure were observed.
Fig. S4. Model of the MPTP.

REFERENCES AND NOTES

1. M. Crompton, The mitochondrial permeability transition pore and its role in cell death. *Biochem. J.* **341**, 233–249 (1999).
2. A. C. Schinzel, O. Takeuchi, Z. Huang, J. K. Fisher, Z. Zhou, J. Rubens, C. Hetz, N. N. Danial, M. A. Moskowitz, S. J. Korsmeyer, Cyclophilin D is a component of mitochondrial permeability transition and mediates neuronal cell death after focal cerebral ischemia. *Proc. Natl. Acad. Sci. U.S.A.* **102**, 12005–12010 (2005).
3. S.-B. Ong, P. Samangouei, S. B. Kalkhoran, D. J. Hausenloy, The mitochondrial permeability transition pore and its role in myocardial ischemia reperfusion injury. *J. Mol. Cell. Cardiol.* **78**, 23–34 (2015).
4. H. Du, S. S. Yan, Mitochondrial permeability transition pore in Alzheimer's disease: Cyclophilin D and amyloid beta. *Biochim. Biophys. Acta* **1802**, 198–204 (2010).
5. D. P. Millay, M. A. Sargent, H. Osinska, C. P. Baines, E. R. Barton, G. Vuagniaux, H. L. Sweeney, J. Robbins, J. D. Molkentin, Genetic and pharmacologic inhibition of mitochondrial-dependent necrosis attenuates muscular dystrophy. *Nat. Med.* **14**, 442–447 (2008).
6. M. Zoratti, I. Szabò, The mitochondrial permeability transition. *Biochim. Biophys. Acta* **1241**, 139–176 (1995).
7. P. Bernardi, R. Colonna, P. Costantini, O. Eriksson, E. Fontaine, F. Ichas, S. Massari, A. Nicolli, V. Petronilli, L. Scorrano, The mitochondrial permeability transition. *Biofactors* **8**, 273–281 (1998).
8. A. P. Halestrap, What is the mitochondrial permeability transition pore? *J. Mol. Cell. Cardiol.* **46**, 821–831 (2009).
9. J. Karch, J. D. Molkentin, Identity of the elusive mitochondrial permeability transition pore: What it might be, what it was, and what it still could be? *Curr. Opin. Physiol.* **3**, 57–62 (2018).
10. A. P. Halestrap, A. M. Davidson, Inhibition of Ca^{2+}–induced large-amplitude swelling of liver and heart mitochondria by cyclosporin is probably caused by the inhibitor binding to mitochondrial-matrix peptidyl-prolyl *cis-trans* isomerase and preventing it interacting with the adenine nucleotide translocase. *Biochem. J.* **268**, 153–160 (1990).
11. K. Woodfield, A. Rück, D. Brdiczka, A. P. Halestrap, Direct demonstration of a specific interaction between cyclophilin-D and the adenine nucleotide translocase confirms their role in the mitochondrial permeability transition. *Biochem. J.* **336**, 287–290 (1998).
12. A. P. Halestrap, C. Brenner, The adenine nucleotide translocase: A central component of the mitochondrial permeability transition pore and key player in cell death. *Curr. Med. Chem.* **10**, 1507–1525 (2003).
13. A. P. Halestrap, Dual role for the ADP/ATP translocator? *Nature* **430**, 984 (2004).
14. A. Rück, M. Dolder, T. Wallimann, D. Brdiczka, Reconstituted adenine nucleotide translocase forms a channel for small molecules comparable to the mitochondrial permeability transition pore. *FEBS Lett.* **426**, 97–101 (1998).
15. N. Brustovetsky, M. Klingenberg, Mitochondrial ADP/ATP carrier can be reversibly converted into a large channel by Ca^{2+}. *Biochemistry* **35**, 8483–8488 (1996).
16. N. Brustovetsky, M. Tropschug, S. Heimpel, D. Heidkämper, M. Klingenberg, A large Ca^{2+}–dependent channel formed by recombinant ADP/ATP carrier from *Neurospora crassa* resembles the mitochondrial permeability transition pore. *Biochemistry* **41**, 11804–11811 (2002).
17. J. E. Kokoszka, K. G. Waymire, S. E. Levy, J. E. Sligh, J. Cai, D. P. Jones, G. R. MacGregor, D. C. Wallace, The ADP/ATP translocator is not essential for the mitochondrial permeability transition pore. *Nature* **427**, 461–465 (2004).
18. C. H. Lim, T. Hamazaki, E. L. Braun, J. Wade, N. Terada, Evolutionary genomics implies a specific function of *Ant4* in mammalian and anole lizard male germ cells. *PLOS ONE* **6**, e23122 (2011).
19. M. Bonora, A. Bononi, E. De Marchi, C. Giorgi, M. Lebiedzinska, S. Marchi, S. Patergnani, A. Rimessi, J. M. Suski, A. Wojtala, M. R. Wieckowski, G. Kroemer, L. Galluzzi, P. Pinton, Role of the c subunit of the F_O ATP synthase in mitochondrial permeability transition. *Cell Cycle* **12**, 674–683 (2013).
20. V. Giorgio, S. von Stockum, M. Antoniel, A. Fabbro, F. Fogolari, M. Forte, G. D. Glick, V. Petronilli, M. Zoratti, I. Szabó, G. Lippe, P. Bernardi, Dimers of mitochondrial ATP synthase form the permeability transition pore. *Proc. Natl. Acad. Sci. U.S.A.* **110**, 5887–5892 (2013).
21. K. N. Alavian, G. Beutner, E. Lazrove, S. Sacchetti, H.-A. Park, P. Licznerski, H. Li, P. Nabili, K. Hockensmith, M. Graham, G. A. Porter Jr., E. A. Jonas, An uncoupling channel within the c-subunit ring of the F_1F_O ATP synthase is the mitochondrial permeability transition pore. *Proc. Natl. Acad. Sci. U.S.A.* **111**, 10580–10585 (2014).
22. J. He, J. Carroll, S. Ding, I. M. Fearnley, J. E. Walker, Permeability transition in human mitochondria persists in the absence of peripheral stalk subunits of ATP synthase. *Proc. Natl. Acad. Sci. U.S.A.* **114**, 9086–9091 (2017).
23. J. He, H. C. Ford, J. Carroll, S. Ding, I. M. Fearnley, J. E. Walker, Persistence of the mitochondrial permeability transition in the absence of subunit c of human ATP synthase. *Proc. Natl. Acad. Sci. U.S.A.* **114**, 3409–3414 (2017).
24. W. Zhou, F. Marinelli, C. Nief, J. D. Faraldo-Gómez, Atomistic simulations indicate the c-subunit ring of the F_1F_o ATP synthase is not the mitochondrial permeability transition pore. *eLife* **6**, e23781 (2017).
25. J. E. Kokoszka, K. G. Waymire, A. Flierl, K. M. Sweeney, A. Angelin, G. R. MacGregor, D. C. Wallace, Deficiency in the mouse mitochondrial adenine nucleotide translocator isoform 2 gene is associated with cardiac noncompaction. *Biochim. Biophys. Acta* **1857**, 1203–1212 (2016).
26. J. V. Brower, C. H. Lim, M. Jorgensen, S. P. Oh, N. Terada, Adenine nucleotide translocase 4 deficiency leads to early meiotic arrest of murine male germ cells. *Reproduction* **138**, 463–470 (2009).
27. T. Nakagawa, S. Shimizu, T. Watanabe, O. Yamaguchi, K. Otsu, H. Yamagata, H. Inohara, T. Kubo, Y. Tsujimoto, Cyclophilin D-dependent mitochondrial permeability transition regulates some necrotic but not apoptotic cell death. *Nature* **434**, 652–658 (2005).
28. C. P. Baines, R. A. Kaiser, N. H. Purcell, N. S. Blair, H. Osinska, M. A. Hambleton, E. W. Brunskill, M. R. Sayen, R. A. Gottlieb, G. W. Dorn II, J. Robbins, J. D. Molkentin, Loss of cyclophilin D reveals a critical role for mitochondrial permeability transition in cell death. *Nature* **434**, 658–662 (2005).
29. P. Varanyuwatana, A. P. Halestrap, The roles of phosphate and the phosphate carrier in the mitochondrial permeability transition pore. *Mitochondrion* **12**, 120–125 (2012).
30. J. Karch, J. D. Molkentin, Identifying the components of the elusive mitochondrial permeability transition pore. *Proc. Natl. Acad. Sci. U.S.A.* **111**, 10396–10397 (2014).
31. R. C. Murphy, E. Schneider, K. W. Kinnally, Overexpression of Bcl-2 suppresses the calcium activation of a mitochondrial megachannel. *FEBS Lett.* **497**, 73–76 (2001).
32. S. Martinez-Caballero, L. M. Dejean, M. S. Kinnally, K. J. Oh, C. A. Mannella, K. W. Kinnally, Assembly of the mitochondrial apoptosis-induced channel, MAC. *J. Biol. Chem.* **284**, 12235–12245 (2009).

Acknowledgments: We thank D. C. Wallace (Children's Hospital of Philadelphia) for supplying *Ant1*$^{-/-}$ and *Ant2*-LoxP–targeted mice. We thank G. Hajnoczky for evaluation of the manuscript. **Funding:** This work was supported by a grant from NIH to J.D.M. (R01HL132831), funding from the Howard Hughes Medical Institutes to J.D.M., funding from Fondation Leducq to J.D.M, and the American Heart Association to J.K. (17SDG33661152) and M.J.B (18POST33960216).
Author contributions: J.K., M.J.B., and J.D.M designed the study and wrote the manuscript. J.K., M.J.B., H.K., M.A.S., N.L., and P.M.P performed experiments and analyzed data. N.T. shared previously generated mutant mouse lines. **Competing interests:** The authors declare that they have no competing interests. **Data and materials availability:** All data needed to evaluate the conclusions in the paper are present in the paper and/or the Supplementary Materials. Additional data related to this paper may be requested from the authors.

Submitted 21 December 2018
Accepted 25 July 2019
Published 28 August 2019
10.1126/sciadv.aaw4597

Citation: J. Karch, M. J. Bround, H. Khalil, M. A. Sargent, N. Latchman, N. Terada, P. M. Peixoto, J. D. Molkentin, Inhibition of mitochondrial permeability transition by deletion of the ANT family and CypD. *Sci. Adv.* **5**, eaaw4597 (2019).